Research Square

Preprints are preliminary reports that have not undergone peer review.
They should not be considered conclusive, used to inform clinical practice,
or referenced by the media as validated information.

Targeting polyamine metabolism and eIF5A hypusination in pediatric acute myeloid leukemia

Courtney Jones

courtney.jones@cchmc.org

Cincinnati Children's Hospital Medical Center

Yun Chueh

Cincinnati Children's Hospital Medical Center https://orcid.org/0009-0008-9160-6572

Karina Camacho

Cincinnati Children's Hospital Medical Center

Nha Nhu Le

Cincinnati Children's Hospital Medical Center https://orcid.org/0009-0004-5235-9004

Raveen Illangeswaran

Cincinnati Children's Hospital Medical Center

Anit Tyagi

University of Colorado https://orcid.org/0000-0001-9455-2591

Julie Reisz

University of Colorado Anschutz Medical Campus

Angelo D'Alessandro

University of Colorado Anschutz Medical Campus https://orcid.org/0000-0002-2258-6490

Christina Sexton

CCHMC

Katharine Carter

CCHMC https://orcid.org/0000-0002-6332-1886

Cody Stillwell

CCHMC

Annabelle Anandappa

CCHMC

Linde Miles

Cincinnati Children's Hospital Medical Center https://orcid.org/0000-0003-3578-2842

Amelie Collins

Cincinnati Children's Hospital Medical Center

Kenneth Greis

University of Cincinnati https://orcid.org/0000-0002-5316-3351

Mark Wunderlich

Cincinnati Children's Hospital Medical Center

Nathan Salomonis

Cincinnati Children's Hospital Medical Center https://orcid.org/0000-0001-9689-2469

Article

Keywords:

Posted Date: November 10th, 2026

DOI: https://doi.org/10.21203/rs.3.rs-10568793/v1

License: This work is licensed under a Creative Commons Attribution 4.0 International License.
Read Full License

Additional Declarations: There is **NO** conflict of interest to disclose.

Targeting polyamine metabolism and eIF5A hypusination in pediatric acute myeloid leukemia

Yun Chueh[1,2], Karina Elizabeth Jiménez Camacho[1,2,5], Nha-Nhu Le[1,2], Raveen Stephen Stallon Illangeswaran[1,2,3], Anit Tyagi[4], Julie A. Reisz[4], Angelo D'Alessandro[4], Christina Sexton[1,2], Katharine M Carter[1,2], Cody Stillwell[1,2], Annabelle J. Anandappa[1,2,3], Linde A. Miles[1,2,4,5], Amélie Collins[5,6], Kenneth D. Greis[3,7], Mark Wunderlich[1,2], Nathan Salomonis[1,3,5,8], Courtney L. Jones[1,2,3,5]

[1]Division of Experimental Hematology and Cancer Biology, Cincinnati Children's Hospital Medical Center, Cincinnati, OH, USA

[2]Advanced Leukemia Therapies and Research Center, Cincinnati Children's Hospital, Cincinnati, OH, USA

[3]University of Cincinnati Cancer Center, Cincinnati, OH, USA

[4]Department of Biochemistry and Molecular Genetics, University of Colorado Anschutz Medical Campus; Aurora, CO, USA

[5]Department of Pediatrics, University of Cincinnati, Cincinnati, OH, USA

[6]Division of Neonatology, Cincinnati Children's Hospital Medical Center, Cincinnati, OH, USA

[7]Division of Cancer Biology, University of Cincinnati, College of Medicine, Cincinnati, Ohio, USA.

[8]Division of Biomedical Informatics, Cincinnati Children's Hospital Medical Center, Cincinnati, OH.

Corresponding Author: Courtney L. Jones, Courtney.Jones@cchmc.org

Competing Interests: The authors disclose no competing interest.

Abstract

Pediatric acute myeloid leukemia (AML) is a devasting disease with 5-year survival outcomes of approximately 60%. Therefore, there is an urgent need to develop novel therapies for pediatric AML patients. Numerous studies have demonstrated that cellular metabolism is a key vulnerability in adult AML; however, metabolism in pediatric AML is less robustly characterized, limiting the development of metabolism targeting therapies for pediatric patients. We have previously shown that manipulation of polyamine metabolism offers a therapeutic window to target adult leukemia, but it is not known if pediatric AML is similarly sensitive. Using pediatric AML patient-derived xenograft models, we demonstrate that polyamine metabolism is a pharmacologically targetable vulnerability of pediatric AML cells. Further, depletion of polyamines sensitizes pediatric AML cells to chemotherapy *in vitro* and *in vivo*. Mechanistically, polyamine depletion reduces protein synthesis through decreased hypusination of translational elongation factor eIF5A. Pharmacologic polyamine depletion and inhibition of eIF5A hypusination result in reduced protein synthesis and decreased expression of cell cycle regulatory proteins resulting in a G_1 cell cycle arrest and eventual cell death through apoptosis. In summary, this study reveals polyamine metabolism and hypusination of eIF5A as a vulnerability in pediatric AML that can be targeted using clinically tractable approaches.

Introduction

Pediatric acute myeloid leukemia (AML) is a biologically heterogeneous disease associated with relatively high relapse rates and poor overall survival[1-3]. Significant progress has been made in the identification and functionalization of genetic and epigenetic drivers of pediatric AML[4-7]. Some of these genetic and epigenetic drivers are also present in adult AML patients; however, pediatric AML remains a distinct disease with many unique biological characteristics and vulnerabilities[8].

Over the past two decades, our understanding of cellular metabolism in adult AML expanded substantially, revealing critical metabolic dependencies and novel mechanisms that contribute to therapy resistance[9-12]. In contrast, the metabolic landscape of pediatric AML remains poorly understood. Existing evidence suggests that leukemic cells from both adult and pediatric AML patients exhibit rewired energy metabolism[13] and that these metabolic programs can be shaped by specific oncogenic mutations[14,15]. However, metabolic vulnerabilities in pediatric AML remain largely unexplored. To investigate metabolic vulnerabilities in pediatric AML, we sought to explore a therapeutically targetable pathway shown to be essential in many adult cancers and safe in clinical trials. This approach was chosen because targeting a pathway shown to be safe in adult patients can allow for more rapid clinical translation in a pediatric population.

Polyamines—putrescine, spermidine, and spermine—are aliphatic molecules containing at least two amino groups that exert broad pleiotropic effects on cellular function[16]. They are often positively charged intracellularly and play a critical role in the growth and survival of multiple cancers[17], including adult AML, neuroblastoma, glioma, melanoma, lymphoma, and breast cancer[18-22]. Importantly, polyamine metabolism can be targeted pharmacologically making it a clinically relevant metabolic vulnerability of cancer cells[23,24]. In clinical trials polyamine targeting approaches have been shown to be safe in adult cancer patients[25-29]. In this study, we examined

the essentiality of polyamine metabolism in pediatric AML patient derived xenograft (PDX) specimens revealing a therapeutically tractable metabolic dependency of pediatric AML cells.

Materials and Methods

PDX Cells

Primary pediatric AML specimens were serially transplanted into immune deficient mice (NSG or NSG-S) for a total of 2–3 transplants for each PDX model. The cells were then viably frozen. Table S1 includes patient specimen characteristics when available.

Cell culture

PDX cells were cultured in IMDM medium (Gibco, 12440061) supplemented with 20% heat inactivated fetal bovine serum (FBS; Corning, 35011CV), 100 U/mL penicillin-streptomycin (Gibco, 15140163), 10 ng/mL SCF (PeproTech, 300-07), 10 ng/mL Flt-3 ligand (PeproTech, 300-19), 10 ng/mL TPO (PeproTech, 300-18), 10 ng/mL IL-3 (PeproTech, 200-03), and 10 ng/mL IL-6 (PeproTech, 200-06). MOLM-13 cells were cultured in RPMI 1640 medium (Thermo Scientific, 11875119) supplemented with 20% heat-inactivated fetal bovine serum (FBS; Corning, 35011CV), and 100 U/mL penicillin-streptomycin (Gibco, 15140163).

Chemicals

N^1, N^{11}-Diethylnorspemine (DENSpm) was purchased from Tocris (0468). GC7 (259545) and difluoromethylornithine (DFMO) (D193) were purchased from Sigma-Aldrich. AMXT-1501 (HY-124617A) and cytarabine (HY-13605) were purchased from MedChem Express.

Colony-forming assays

Colony-forming assays were performed using enriched MethoCult medium (STEMCELL Technologies, 04435). Cells were treated with DENSpm (10 μM), DFMO (2.5 mM), AMXT-1501

(400 nM), or DFMO + AMXT-1501 (2.5 mM and 400 nM, respectively) for 24 h. GC7 (50 μM) was added directly to the MethoCult medium. Colonies were counted 14–21 days post-plating.

For MOLM-13 cells, colony-forming assays were performed using classic MethoCult medium (STEMCELL Technologies, 04434). Cells were plated 72 h after puromycin withdrawal. Colonies were counted 7 days post-plating.

Immunoblotting

Cells were lysed in RIPA buffer (Sigma-Aldrich, R0278) supplemented with protease inhibitor cocktail and EDTA (Thermo Scientific, 78438) on ice for 1 h. Lysates were clarified by centrifugation for 20 min at 4°C. Protein concentration was determined using the BCA Protein Assay Kit (Thermo Scientific, 23225). Equal amounts of protein were loaded and resolved on 4–15% precast polyacrylamide gels (Bio-Rad, 4561084) and transferred to LF PVDF membranes (Bio-Rad, 1704274) using the Trans-Blot Turbo Transfer System (Bio-Rad). Membranes were blocked with EveryBlot Blocking Buffer (Bio-Rad, 12010020) for 5 min at room temperature and then probed with primary antibodies against hypusine (1:500; Creative Biolabs, PABL-202), DYKDDDDK tag (1:500; Cell Signaling Technology, 2368S), and GAPDH (1:1000; Santa Cruz Biotechnology, sc-365062) overnight at 4°C. Blots were then incubated with IRDye 680RD anti-mouse IgG (1:20,000; LI-COR Biosciences, 926-68070) or IRDye 800CW anti-rabbit IgG (1:20,000; LI-COR Biosciences, 926-32211) for 1 h at room temperature. Signals were detected using a LI-COR Odyssey imaging system.

Protein synthesis measuring assays

Cells were treated with DENSpm (10 μM), DFMO + AMXT-1501 (2.5 mM and 400 nM, respectively), or GC7 (25–50 μM) for 24 h. Cells were then incubated with 10 μg/mL puromycin dihydrochloride (Gibco, A1113803) for 30 min, followed by staining with PE-Cy7 anti-CD34 (BD Biosciences, 560710) for 20 min. Samples were fixed and permeabilized using the

Cytofix/Cytoperm Fixation/Permeabilization Kit (BD Biosciences, 554714). Cells were subsequently stained with Alexa Fluor 488 anti-puromycin (Sigma-Aldrich, MABE343-AF488) for 1 h and counterstained with DAPI (Sigma-Aldrich, D9542). Samples were analyzed by flow cytometry on a BD FACSymphony.

Cell cycle analysis

Cells were treated with DENSpm (10 μM) or GC7 (50 μM) for 24 h, followed by fixation, permeabilization, and staining using the Click-iT EdU Alexa Fluor 647 Flow Cytometry Assay Kit (Thermo Scientific, C10424). Samples were analyzed by flow cytometry on a BD FACSymphony.

Apoptosis analysis

Cells were treated with DENSpm (10 μM), DFMO (2.5 mM), AMXT-1501 (400 nM), DFMO + AMXT-1501 (2.5 mM and 400 nM, respectively), or GC7 (50 μM) for 48 h. Apoptosis was assessed by FITC Annexin V (BioLegend, 640945) and DAPI (Sigma-Aldrich, D9542) staining. Samples were analyzed by flow cytometry on a BD FACSymphony.

Cell viability assays

Cells were treated with DENSpm (10, 5, 2.5, and 1.25 μM), cytarabine (10, 5, 2.5, and 1.25 μM), or all pairwise combinations of DENSpm and cytarabine at the indicated concentrations for 48 h. Cell viability was determined using the CellTiter-Glo Luminescent Cell Viability Assay Kit (Promega, G7572).

Proteomics

Cells from three PDX samples were treated with DENSpm (10 μM) or GC7 (50 μM) for 24 h. A total of 2 x 10^5 cells were collected, washed twice with PBS, pelleted, and stored at −80°C until analysis. Proteomics analysis was performed by the University of Cincinnati Proteomics

Laboratory (RRID:SCR_025895). Sample preparation included lysis of the frozen cell pellets followed by reduction, alkylation, and digestion with LysC/Trypsin and sample clean-up, all using the EasyPep sample preparation kit (Thermo Scientific, A40006) protocol. A 30,000 cell equivalent of the recovered peptides (15% of the total) from each sample was analyzed by nanoFlow Liquid Chromatography-Mass Spectrometry followed by a Label Free Quantitation (LFQ) workflow on a Dionex Ultimate 3000 RSLCnano coupled to a Thermo Orbitrap Eclipse mass spectrometry system. Data were collected using Xcaliber 4.3 software (Thermo Scientific) with LFQ comparative profiling of proteins detected from each sample group achieved using Proteome Discoverer 3.0 (Thermo Scientific) with a search against a Uniprot Homo sapiens database (UP000005640). Full details of the mass spectrometry and data analysis parameters are available in Bennett, *et al*, 2023[30]. Additional data processing and statistical analysis was performed using metaboanalyst. KEGG pathway analysis was performed using ShinyGO[31]. PCA plots were generated using Biomni[32].

RNA sequencing and ribosome sequencing

Cells were treated with DENSpm (10 μM) or GC7 (50 μM) for 24 h. For RNA sequencing, total RNA was extracted from 1 x 10^6 cells using TRIzol reagent (Thermo Scientific, 15596026). For ribosome sequencing, 1 x 10^7 cells were treated with cycloheximide (0.1 mg/mL; Thermo Scientific, AAJ66004XF) before collection. Samples were stored at −80°C until library preparation and sequencing. Library preparation and sequencing were performed by CD Genomics. For RNA sequencing, mRNA was purified, fragmented, and converted into double-stranded cDNA, followed by adapter ligation, library amplification, quality assessment, and sequencing on the MGI DNBSEQ-T7 platform.

For ribosome sequencing, ribosome-protected fragments (RPFs) were generated by RNase digestion, isolated by size-exclusion chromatography, depleted of ribosomal RNA,

phosphorylated, and used for library preparation, followed by quality assessment and sequencing on the Illumina NovaSeq X Plus platform.

Ribosome Sequencing and Matched RNA Sequencing Analysis

Ribo-Seq FASTQ files were processed using the nf-core/riboseq pipeline (version 1.2.0) executed with Nextflow on the Cincinnati Children's Hospital research high performance LSF computing cluster using Singularity containers. Quality control was performed using FastQC version 0.12.1 and validated using fq version 0.12.0. Illumina small-RNA adapters were removed using Trim Galore! version 0.6.10 and Cutadapt version 4.9, with a Phred quality threshold of 20, maximum error rate of 0.1, minimum adapter overlap of 1 nucleotide, and minimum retained read length of 18 nucleotides. Ribosomal RNA reads were depleted using SortMeRNA version 4.3.7 in paired-read mode against the eight default nf-core Rfam and SILVA default ribosomal RNA reference databases. Remaining ribosome-protected fragments were aligned using STAR version 2.7.11b to the Illumina iGenomes UCSC hg38 human reference genome and corresponding gene annotation. The STAR genome index was generated with annotated splice junctions and an sjdbOverhang of 100. Alignment was performed in basic two-pass mode with end-to-end alignment, a minimum annotated splice-junction overhang of 1 nucleotide, and a maximum of 20 reported alignments per read.

Matched paired-end bulk RNA-sequencing libraries were aligned to the human GRCh38 reference genome using STAR version 2.4.0h in a two-pass, sample-specific alignment. During the first pass, splice-junction evidence was collected using a maximum intron length of 500 kb, maximum mate gap of 1 Mb, and a maximum of 20 reported alignments per read. The resulting splice-junction coordinates were used to construct a sample-specific STAR genome index, followed by a second alignment to produce coordinate-sorted BAM files. Alignments retained standard mapping, mismatch, alignment-score, and splice-strand attributes.

Gene-level abundance was quantified from the resulting Ribo-seq and RNA-seq BAM files using featureCounts version 2.0.6. Reads were assigned to Ensembl genes (EnsMart91 human database) by AltAnalyze. Paired-end fragments were counted once per gene using -p --countReadPairs, with forward-stranded counting (-s 1). Gene lengths were defined as the union of nonredundant exonic bases assigned to each gene. Raw fragment counts and reads per kilobase per million mapped fragments (RPKM) were used for downstream quantification.

Gene-expression matrices were analyzed using AltAnalyze version 2.1.4. Ribo-seq and matched RNA-seq datasets were analyzed separately using identical sample and treatment-group definitions. Differential gene expression was evaluated using moderated t-tests, and regulated genes were defined using a minimum 1.5-fold change and an empirical Bayes t-test $P < 0.05$. Principal-component analysis, MarkerFinder and hierarchical clustering in AltAnalyze were used to assess sample relationships and treatment-associated expression patterns. Replicate-associated marker genes were identified using MarkerFinder, and Gene Ontology and pathway enrichment analyses were performed with GO-Elite using Fisher's exact-test over-representation analysis and a minimum enrichment z-score of 1.96.

Metabolomics

Cells were treated with DENSpm (10 μM), DFMO (2.5 mM), AMXT-1501 (400 nM), or DFMO + AMXT-1501 (2.5 mM and 400 nM, respectively) for 24 h. Cells were collected in four technical replicates (1×10^5 cells per replicate). Each replicate was washed twice with cold PBS and stored at −80°C until analysis. Metabolomics analysis was performed at the University of Colorado School of Medicine Metabolomics Core as previously described[18].

Gene knockdown and overexpression

Non-targeting control shRNA and shRNA targeting the 3′ untranslated region (3′UTR) of eIF5A (MilliporeSigma, TRCN0000062548) were used for knockdown experiments. Lentiviral expression constructs encoding empty vector control, wild-type eIF5A (WT-eIF5A), or a hypusination-defective mutant of eIF5A (K50R-eIF5A) were purchased from GeneCopoeia. The eIF5A constructs correspond to human eIF5A (NM_001143761.1) with an N-terminal Flag tag and were cloned into the lentiviral pReceiver-Lv173 vector under the control of the EF1α promoter, with an IRES-mCherry reporter. Lentiviruses were produced by the Cincinnati Children's Hospital Medical Center Viral Vector Facility.

MOLM-13 cells were transduced with lentiviruses encoding empty vector, WT-eIF5A or K50R-eIF5A in the presence of polybrene (8 μg/mL). 72 h after transduction, cells were expanded in culture, and mCherry-positive cells were isolated by cell sorting to establish stable overexpression populations. These cells were subsequently transduced with lentivirus encoding either non-targeting control shRNA or eIF5A 3′UTR-targeting shRNA in the presence of polybrene (8 μg/mL). Following transduction, cells were selected with puromycin (1.5 μg/mL) for 48 h. Knockdown and overexpression efficiencies were confirmed by immunoblotting.

In vivo drug treatment

PDX cells were engrafted into NRGS mice (NOD.Cg-Rag1tm1MomIL2rgtm1WjlTg(CMV-IL3,CSF2,KITLG)1Eav/J) following busulfan conditioning. Treatments began on day 26 of engraftment and consisted of 2 weeks of DENSpm (60 mg/kg, once daily Monday–Friday, IP injection) and/or Daunorubicin (2 mg/kg, IV injection) combined with AraC (50 mg/kg, IV injection) once daily for the first 3 days of treatments.

Results

Polyamine depletion targets pediatric AML cells *in vitro* and *in vivo*

To determine if pediatric AML cells are dependent on polyamines for their survival, we depleted polyamines using two complementary pharmacologic approaches and measured polyamine levels and colony-forming potential of pediatric AML patient derived xenograft (PDX) models. The PDX models we used in this study were each derived from relapsed/refractory (R/R) AML patients (Table S1), as these patients are often resistant to currently used therapies and have the greatest need for new therapeutic approaches. First, we treated cells with N^1,N^{11}-diethylnorspermine (DENSpm) which results in acetylation and cellular export of spermidine and spermine. Metabolite abundance in PDX cells was quantified by mass spectrometry metabolomics to determine the effect of DENSpm. Intracellular levels of putrescine, spermidine, and spermine were drastically reduced upon DENSpm treatment (Fig. S1A), indicating effective depletion of polyamines. DENSpm abundance was also detected in treated PDX cells (Fig. S1A), confirming cellular uptake. Polyamine depletion through DENSpm treatment resulted in significant abrogation of the colony-forming potential of all eight pediatric AML PDX specimens examined (Fig. 1A and Fig. S1B).

To complement these studies, we reduced polyamine abundance by targeting both polyamine biosynthesis and cellular import. Previous studies have demonstrated that inhibition of only one of these pathways can result in compensation from the other, but combinatorial approaches can result in increased anti-tumor effects in pre-clinical models[20]. Therefore, we performed studies with individual inhibitors and their combination in AML cells. Inhibition of polyamine biosynthesis with difluoromethylornithine (DFMO), an ornithine decarboxylase 1 (ODC1) inhibitor, together with

reduction of polyamine transport using AMXT-1501, an inhibitor of the polyamine transporter SLC3A2, reduced intracellular levels of putrescine and spermidine, but not spermine, in pediatric AML PDX cells (Fig. S1C). Interestingly, DFMO treatment alone was sufficient to significantly reduce putrescine and spermidine levels in pediatric AML PDX cells. AMXT-1501 alone did not significantly reduce polyamine levels but did result in elevated putrescine levels, suggesting a compensation mechanism occurs upon polyamine transport inhibition in pediatric AML. Notably, the combination of DFMO and AMXT-1501 resulted in a greater reduction in spermidine levels compared to individual treatments (Fig. S1C). Colony-forming potential was reduced in seven of eight AML PDX models upon combination treatment with DFMO and AMXT-1501 (Fig. 1B and Fig. S1D). Interestingly, we observed reduced colony formation in five of the eight AML PDX models upon DFMO only treatment and one AML PDX model upon AMXT-1501 only treatment. However, combination treatment often resulted in a greater reduction in colony-forming potential compared to DFMO alone, consistent with the degree of polyamine reduction observed by mass spectrometry. Finally, we determined the effects of polyamine depletion in pediatric AML cells *in vivo*. PDX cells derived from two pediatric AML patients were transplanted into NSG-S mice, and mice were treated with DENSpm (60 mg/kg) 5 days per week for 2 weeks (Fig. 1C). DENSpm treatment significantly reduced leukemic burden in the bone marrow but failed to fully eradicate the disease. Importantly, we have previously demonstrated polyamine targeting approaches do not target normal hematopoietic cells *in vitro* or *in vivo*[18] and polyamine depletion showed limited toxicity in clinical trials[25-27], suggesting that a therapeutic window exists to target polyamines in pediatric AML cells. These results suggest that polyamines are important for the survival of pediatric AML cells but targeting them alone is insufficient to eliminate pediatric AML cells.

Polyamine depletion reduces eIF5A-mediated protein synthesis in pediatric AML

Since polyamine depletion alone will not fully eradicate pediatric AML cells, we next sought to determine the mechanism by which polyamine depletion targets pediatric AML with the goal of

developing rational combination therapy strategies. Polyamines have pleiotropic cellular functions including regulating DNA structure, gene expression, ion channel activity, cell growth, and protein synthesis[33]. Our previous work demonstrated that polyamines are essential for protein synthesis in adult AML[18]; therefore, we first looked at the consequences of polyamine depletion on protein synthesis. Polyamines are known to regulate protein synthesis through the hypusination of eIF5A, a translation elongation factor[34-36]. Interestingly, eIF5A is the only known protein to be hypusinated. In the two-step hypusination process, the enzyme deoxyhypusine synthase (DHS) transfers the 4-aminobutyl moiety from spermidine to the amino group of lysine 50 on eIF5A resulting in a deoxyhypusine intermediate. Deoxyhypusine hydroxylase (DOHH) then hydroxylates deoxyhypusine to hypusine[37]. Hypusination of eIF5A promotes efficient protein elongation, particularly in proteins that contain amino acid sequences that are difficult to translate, such as polyproline motifs[35]. Consistent with the literature, polyamine depletion using DENSpm or DFMO with AMXT-1501 in $CD34^+$ pediatric AML PDX models resulted in reduced eIF5A hypusination (Fig. S2A) and reduced protein synthesis levels (Fig. 2A). To mechanistically interrogate if hypusination of eIF5A was essential for AML cell survival we knocked down endogenous eIF5A using an shRNA targeting the three-prime untranslated region of eIF5A, reconstituted the cells with wild-type or a loss of hypusination mutant eIF5A (K50R) and measured colony-forming potential in the MOLM-13 AML cell line (Fig. 2B and 2C). Knockdown of eIF5A resulted in a significant reduction in the colony-forming potential of AML cells, which was rescued by expression of the wild-type but not K50R mutant eIF5A. These data demonstrate that eIF5A hypusination is essential for AML cell colony-forming ability. To determine if hypusination is essential in pediatric AML PDX cells, we inhibited DHS using the tool compound GC7 and measured eIF5A hypusination, protein synthesis, and colony-forming potential. DHS inhibition resulted in reduced eIF5A hypusination (Fig. S2B) and protein synthesis (Fig. 2D) in three pediatric AML PDX models. Further, DHS inhibition striking reduced the colony-forming potential of all eight pediatric AML PDX models (Fig. 2E and Fig. S2C), demonstrating that pediatric AML

cells are dependent on the eIF5A hypusination pathway. Consistent with prior studies[18], GC7 treatment resulted in a modest 30% reduction in colony forming potential of normal HSPCs, demonstrating that pediatric AML cells are more dependent on eIF5A hypusination than normal cord blood HSPCs (Fig. 2F). Altogether, these data suggest that inhibition of eIF5A hypusination is an effective strategy to target pediatric AML cells while not harming normal hematopoietic cells.

Polyamine depletion and eIF5A hypusination inhibition reduce the expression of cell cycle proteins

To define the mechanism underlying the effects of polyamine depletion and eIF5A hypusination inhibition on pediatric AML cells, we sought to first identify the proteins downregulated upon polyamine depletion and inhibition of eIF5A hypusination. We treated three pediatric AML PDX samples with DENSpm or GC7 for 24 hours and measured global protein levels using mass spectrometry (Fig. 3A). A total of 2,749 proteins were detected in the three PDX specimens albeit with notable heterogeneity among the AML specimens. Indeed, principal component analysis (PCA) revealed that the samples clustered by patient specimen and not treatment group (Fig S3A). Polyamine depletion and eIF5A hypusination inhibition largely resulted in reduced protein levels with few proteins showing elevated expression (Fig. 3B). Paired t-test analysis revealed that 153 and 149 proteins were significantly changed upon DENSpm and GC7 treatment respectively with 47 proteins showing conserved changes between DENSpm and GC7 (Fig. 3C). Of the 47 proteins with conserved changes, 45 had reduced expression and two proteins had elevated expression upon DENSpm and GC7 treatment (Fig. 3D). KEGG pathway analysis of the shared proteins revealed that proteins involved in DNA replication and the cell cycle were the most enriched upon DENSpm and GC7 treatment (Fig. 3E). Notably, proteins central to cell cycle and DNA replication regulation including CDK1 and MCM protein family members (MCM4, MCM6, and MCM7) were all downregulated. Altogether, these data suggest that polyamine depletion and

inhibition of eIF5A hypusination in pediatric AML specimens results in reduced expression of proteins that regulate the cell cycle.

Cell cycle mRNAs have reduced translation upon polyamine depletion and eIF5A hypusination inhibition

To determine if changes in cell cycle protein expression were a result of reduced transcription or translation, we performed paired ribosome profiling and RNA-sequencing analysis in a PDX specimen treated with DENSpm and GC7. Ribosome sequencing analysis revealed differential ribosome occupancy of 3,402 and 3,801 mRNAs upon DENSpm and GC7, respectively (Fig S4A). Similar to our proteomic studies, KEGG pathway analysis revealed an enrichment for DNA replication and cell cycle mRNAs (Fig S4B). Consistent with the pathway analysis, marker gene analysis showed that cell cycle and DNA replication mRNAs were downregulated upon polyamine depletion and eIF5A hypusination inhibition compared to control cells (Fig S4C). Interestingly, DENSpm and GC7 treatment resulted in a unique pattern of upregulated gene markers (Fig S4C), highlighting that polyamine depletion and eIF5A hypusination inhibition can result in distinctive translational signatures. To determine if cell cycle mRNAs had reduced ribosome occupancy due to a decrease in transcription or translation, we compared the expression of mRNAs in the ribosome sequencing analysis and RNA-sequencing analysis. For this analysis, we chose to use a stringent cutoff to define translation-specific events as ribosome occupancy differences as significance with an adjusted p-value<0.05 and RNA expression differences as significance with a raw p-value>0.05. Consistent with the ribosome-sequencing data, PCA of the differentially translated mRNAs showed that polyamine depletion and eIF5A hypusination resulted in distinct grouping with both DENSpm and GC7 treatment being notably different from vehicle-treated cells while also being different from each other (Fig. 4A). 1664 and 2759 mRNAs were uniquely increased in the ribosome-sequencing analysis upon DENSpm and GC7 treatment, respectively. 1016 and 631 mRNAs were uniquely decreased in the ribosome-sequencing analysis upon

DENSpm and GC7 treatment, respectively (Fig. 4B). Pathway analysis showed that mRNAs related to the cell cycle had reduced translation compared to vehicle control upon DENSpm and GC7 treatment (Fig. 4C). A total of 23 cell cycle related pathways were significantly reduced upon DENSpm treatment out of a total of 273 significantly reduced gene ontology terms. Similarly, 11 cell cycle related pathways were significantly reduced upon GC7 treatment out of a total of 212 significantly reduced gene ontology terms. Interestingly, the same cell cycle proteins downregulated in the proteomics analysis had decreased ribosome occupancy and mRNA expression (Fig S5A and S5B). These data demonstrate that polyamine depletion and eIF5A hypusination reduce cell cycle related translation in pediatric AML cells, but the reduced protein level observed by mass spectrometry were primarily driven by transcriptional changes.

Polyamine depletion and eIF5A hypusination inhibition result in cell cycle arrest

To determine if changes in the expression of cell cycle proteins resulted in a functional change in the cell cycle, we measured EdU incorporation upon polyamine depletion or eIF5A-hypusination inhibition in three pediatric AML PDX specimens. Following a 24-hour treatment with DENSpm and GC7, cells accumulated in the G_o-G_1 phase of the cell cycle, which resulted in a significant reduction in AML cells within the S phase of the cell cycle in all 3 AMLs tested (Fig. 5A and 5B). These data indicate that polyamine depletion and eIF5A-hypusination loss result in cell cycle arrest at the G_o-G_1 stage. As cell cycle and protein synthesis are commonly linked processes, we next sought to determine if the reduction in protein synthesis was occurring at each stage of the cell cycle or only within cells at the G_o-G_1 stage. We separated cells into G_o-G_1 and G_2-M-S phases and then measured the levels of puromycin incorporation into newly synthesized proteins upon DENSpm and GC7 treatment, as previously described[38]. These data showed that polyamine depletion and eIF5A hypusination inhibition resulted in a reduction in protein synthesis across the cell cycle stages (Fig. 5C). Finally, to determine if polyamine depletion and eIF5A hypusination inhibition-induced cell cycle arrest resulted in apoptosis, we measured Annexin V and DAPI

positive cells 48 hours post-treatment (Fig. 5D). DENSpm and GC7 treatment resulted in a striking induction in apoptosis in three pediatric AML PDX models. These data contrast with what we have previously observed in adult AML specimens[18]. In adult AML, polyamine depletion causes myeloid differentiation and loss of stemness and does not alter the cell cycle or result in rapid apoptosis[39]. To examine if polyamine depletion could cause differentiation in pediatric AML PDX models, we treated with cells with low dose DENSpm or GC7 and measured the expression of CD15, CD14, and CD11b in colony forming unit assays, as we had previously done in adult AML[18]. We did not observe any significant increase in myeloid markers in the pediatric AML specimens (Fig. S6). These data alone cannot rule out the potential for myeloid cell differentiation to contribute to cell death in pediatric leukemia upon polyamine depletion. However, altogether the data support the mechanism that pediatric AML specimens require polyamine metabolism for regulation of the cell cycle which when disturbed results in apoptosis.

Polyamine deprivation sensitizes pediatric AML cells to chemotherapy

Among common front-line therapy options for pediatric AML patients, cytarabine is a pyrimidine nucleoside analog that results in cell cycle arrest[40]. Moreover, inhibition of cell cycle regulation has been shown to sensitize AML cells to cytarabine[41,42]. Therefore, we hypothesized that polyamine depletion would have enhanced efficacy in combination with cytarabine. We measured cell viability of three pediatric AML PDX specimens upon treatment with lower-dose DENSpm, cytarabine or the combination (Fig. 6A). Combination therapy resulted in a significantly lower cell viability compared to either treatment alone. Next, we performed synergy calculations to determine if the combinatorial effect was indeed synergistic. In all PDX specimens examined, the combination therapy was found to be synergistic, regardless of the model (Bliss or Lowry) used to calculate synergy (Fig. S7). Next, we determined if the combination treatment resulted in reduced colony-forming potential of pediatric AML PDX specimens. For these experiments, we treated PDX cells with low-dose cytarabine and DENSpm and measured colony-forming ability

two weeks post-plating. Combination treatment resulted in a greater reduction in colony-forming potential compared to single-agent treatment (Fig. 6B). Finally, we examined the efficacy of DENSpm in combination with standard of care chemotherapy, cytarabine and daunorubicin, *in vivo*. Mice were transplanted with AML2, treated for two weeks, and bone marrow burden was monitored through bone marrow aspirations. Chemotherapy alone and DENSpm with chemotherapy significantly reduced leukemia burden 45 days after treatment with a trend of lower leukemic burden in the combination therapy (Fig. 6C). The combination therapy further reduced the leukemia burden in mice compared to chemotherapy alone 56 days post treatment (Fig. 6C). At this later timepoint the majority of control mice had died from leukemia; therefore, leukemia burden could not be assessed in those mice. Importantly, the overall survival of mice transplanted with AML2 was significantly longer upon treatment with any therapy compared to vehicle treatment and was significantly extended by the combination treatment compared to chemotherapy alone (Fig. 6D), suggesting combining chemotherapy with a polyamine-depleting strategy could improve outcomes for pediatric AML patients.

Discussion:

Despite the significant advancement in our knowledge of adult AML cell metabolism, little is known about cellular metabolism in pediatric AML. Much of what we know about metabolism in pediatric AML cells has been inferred from adult AML studies with only a handful of studies directly analyzing metabolism in pediatric AML patient samples or pediatric PDX models. In pediatric AML specimens, changes in metabolite levels have been determined to be altered depending on the genetic drivers of the disease. Specifically, pediatric AML patients harboring a FLT-ITD translocation have a distinct cellular and plasma metabolism compared to wild type patients[14]. Electron transport chain (ETC) complex II and V activity are elevated in pediatric AML cells compared to aged-matched normal bone marrow controls[43], but this increased activity does not correlate with disease biology or clinical outcomes[43]. Overall, there is a critical need for more

studies to examine cellular metabolism in pediatric AML and identify novel metabolic vulnerabilities within this disease.

In this study, we examined the essentiality of polyamine metabolism, a clinically targetable pathway downstream of arginine. We used two complementary polyamine-depleting strategies. First, we used DENSpm, a polyamine analog previously shown to be safe in metastatic breast cancer, lung cancer, and hepatocellular carcinoma clinical trials[25-27]. In addition, we used the polyamine biosynthesis inhibitor DFMO with the polyamine uptake inhibitor AMXT-1501. DFMO has been shown to be safe in clinical trials but lacks efficacy, likely due to compensation through polyamine uptake[20,22,28,29]. AMXT-1501 synergizes with DFMO in preclinical models of diffuse intrinsic pontine glioma[20] which resulted in the initiation of a Phase 1B/2A trial that included patients 12 years and older (NCT05500508). This trial was terminated, and reformulation of DFMO from IV to capsule administration was required due to safety concerns. Our study suggests that targeting polyamine metabolism could represent a promising strategy in pediatric AML, especially in combination with chemotherapy, which could be clinically meaningful if the therapeutics are well-tolerated post reformulation. Our study exclusively used relapsed/refractory AML specimens (Table S1) because these are the patients with the highest need for novel therapies and would likely be the first to be eligible for a clinical trial. It remains unknown if treatment-naive pediatric AML cells would respond similarly to polyamine depletion or eIF5A hypusination inhibition.

Mechanistically, our data demonstrate that polyamine metabolism is essential in pediatric AML cells through their role in regulating eIF5A hypusination-mediated mRNA translation and protein synthesis. Polyamine depletion reduces the synthesis of proteins important for the regulation of the cell cycle and therefore results in cell cycle arrest. Many of the proteins with reduced expression were not changed in the ribosome-sequencing data, suggesting that the reduction in

protein expression could be a secondary consequence of the effects of DENSpm and GC7 resulting from differential translation of the identified cell cycle related mRNAs. The mRNAs with reduced translation driving cell cycle arrest remain to be elucidated.

A similar G_1 arrest upon polyamine depletion and eIF5A hypusination inhibition has been shown in primary CD8+ T cell lymphocytes[44]. Interestingly, reduced levels of CDK1 were observed in T cells upon GC7 and DFMO treatment[44], consistent with what we observed in pediatric AML specimens upon GC7 and DENSpm treatment suggesting that some targets are likely conserved across some cell types. However, GC7 treatment in CD8+ T lymphocytes did not induce cell death[44]. Polyamine depletion and eIF5A hypusination inhibition induced G_o-G_1 arrest which contributes to apoptosis has also been noted in lymphoma[17]. These data indicate that the observed cell cycle arrest contributes to cell death in some hematologic malignancies but not normal lymphocytes. Interestingly, changes in the cell cycle were not observed in diffuse intrinsic pontine gliomas or adult AML LSCs[18,20] suggesting that the mechanism by which polyamine depletion targets cancer cells may be unique depending on the tumor type and cell population.

Overall, our study has revealed that pediatric AML cells rely on polyamine metabolism and hypusination of eIF5A for survival. This is one of the very few studies that have examined cellular metabolism in pediatric AML PDX models. One limitation of the study is that we relied on the use of PDX models, and primary AML specimens were not analyzed. This is often a limitation when working with pediatric AML, due to the low cell numbers that can be collected from these patients. In addition, examining the off-target metabolic effects of polyamine-depleting therapies[45] should be explored in greater detail in pediatric AML. Finally, polyamine-targeting therapies will need to be further explored in children to ensure this is a safe tolerable therapy. Despite these limitations, our work lays the foundation for future studies to examine the translational potential of polyamine targeting therapy in pediatric AML.

Acknowledgements: This study was funded by Blood Cancer United Specialized Center of Research grant (L.A.M. and C.L.J.); the Rally Foundation, grant 24CDN01 (C.L.J.); The V Foundation, grant V2024-012 (C.L.J.); Alex's Lemonade Stand Foundation, grant 1330583 (C.L.J.); Cincinnati Children's Hospital Medical Center Trustee Award (L.A.M. and C.L.J.); Cancer Free Kids (K.E.J.C); Blood Cancer United Career Development Program Fellow Award (R.S.S.I.); Damon Runyon Physician-Scientist Training Award (A.J.A, PST-49-25); The American Society of Hematology Scholars Grant (L.A.M. and C.L.J); University of Colorado Cancer Center support grant (P30CA046934; A.D. and J.A.R.); NCI, NIH grant R50 CA211404 (M.W.); National Institute of Diabetes and Digestive and Kidney Diseases, NIH grant U54DK126108; and NCI, NIH Shared Instrumentation Grant (S10OD026717) for the UC Proteomics Laboratory (K.D.G.), NIH grant R37CA291896 (C.L.J.).

Author Contributions: Y.C. was responsible for performing experiments, analyzing data, generating figures, and writing and editing the manuscript. K.E.J.C. was responsible for performing experiments, analyzing data, generating figures, and writing and editing the manuscript. N.N.L. was responsible for performing experiments, analyzing data, generating figures, and editing the manuscript. R.S.S.I performed experiments, generated figures, and reviewed the manuscript, A.T. performed experiments and reviewed the manuscript. J.A.R was responsible for analyzing polyamine levels upon drug treatment, writing and editing the manuscript. A.D. was responsible for analyzing polyamine levels upon drug treatment, writing and editing the manuscript. C.S. was responsible for performing animal experiments. K.M.C was responsible for performing animal experiments. C.S. was responsible for performing animal experiments. A.J.A. assisted with cell cycle analysis and reviewed the manuscript, A.C. provided UCB samples and advised on normal HSPC experiments. L.A.M. advised on experimental design, wrote and edited the manuscript, K.D.G. was responsible for performing and overseeing proteomics analysis, writing and editing the manuscript. M.W. was responsible for designing,

performing and overseeing all animal experiments, analyzing data, writing and editing the manuscript. N.S. was responsible for analyzing ribosome sequencing data, generating figures, writing and editing the manuscript. C.L.J conceptualized the project, oversaw the project development, analyzed data, and wrote and edited the manuscript.

Competing Interests: Authors declare no competing financial interests in relation to the work described.

Data Availability Statement: The proteomics data is available on ProteomeXchange (Project Accession Number: PDX080990, Token FeVj05XafeFw). Ribosome sequencing data is available on GEO (GSE342172). All other data will be made available by the corresponding author upon reasonable request.

References

1 Zwaan, C. M. *et al.* Diagnosis and management of AML in pediatric patients: consensus recommendations from an international expert panel. *Blood* **147**, 1532-1561 (2026). https://doi.org/10.1182/blood.2024027904

2 Egan, G. & Tasian, S. K. Relapsed pediatric acute myeloid leukaemia: state-of-the-art in 2023. *Haematologica* **108**, 2275-2288 (2023). https://doi.org/10.3324/haematol.2022.281106

3 Egan, G. & Tasian, S. K. Precision medicine for high-risk gene fusions in pediatric AML: a focus on KMT2A, NUP98, and GLIS2 rearrangements. *Blood* **145**, 2574-2586 (2025). https://doi.org/10.1182/blood.2024026598

4 Shiba, N. *et al.* Whole-exome sequencing reveals the spectrum of gene mutations and the clonal evolution patterns in paediatric acute myeloid leukaemia. *Br J Haematol* **175**, 476-489 (2016). https://doi.org/10.1111/bjh.14247

5 Newcombe, A. A., Gibson, B. E. S. & Keeshan, K. Harnessing the potential of epigenetic therapies for childhood acute myeloid leukemia. *Exp Hematol* **63**, 1-11 (2018). https://doi.org/10.1016/j.exphem.2018.03.008

6 Ma, X. *et al.* Pan-cancer genome and transcriptome analyses of 1,699 paediatric leukaemias and solid tumours. *Nature* **555**, 371-376 (2018). https://doi.org/10.1038/nature25795

7 Bolouri, H. *et al.* The molecular landscape of pediatric acute myeloid leukemia reveals recurrent structural alterations and age-specific mutational interactions. *Nat Med* **24**, 103-112 (2018). https://doi.org/10.1038/nm.4439

8 Chaudhury, S. *et al.* Age-specific biological and molecular profiling distinguishes paediatric from adult acute myeloid leukaemias. *Nat Commun* **9**, 5280 (2018). https://doi.org/10.1038/s41467-018-07584-1

9 Addanki, S., Kim, L. & Stevens, A. Understanding and Targeting Metabolic Vulnerabilities in Acute Myeloid Leukemia: An Updated Comprehensive Review. *Cancers (Basel)* **17** (2025). https://doi.org/10.3390/cancers17081355

10 Jones, C. L., Inguva, A. & Jordan, C. T. Targeting Energy Metabolism in Cancer Stem Cells: Progress and Challenges in Leukemia and Solid Tumors. *Cell Stem Cell* **28**, 378-393 (2021). https://doi.org/10.1016/j.stem.2021.02.013

11 Mishra, S. K., Millman, S. E. & Zhang, L. Metabolism in acute myeloid leukemia: mechanistic insights and therapeutic targets. *Blood* **141**, 1119-1135 (2023). https://doi.org/10.1182/blood.2022018092

12 O'Brien, C. & Jones, C. L. Unraveling lipid metabolism for acute myeloid leukemia therapy. *Curr Opin Hematol* **32**, 77-86 (2025). https://doi.org/10.1097/moh.0000000000000853

13 Stratmann, S. *et al.* Proteogenomic analysis of acute myeloid leukemia associates relapsed disease with reprogrammed energy metabolism both in adults and children. *Leukemia* **37**, 550-559 (2023). https://doi.org/10.1038/s41375-022-01796-7

14 Stockard, B., Garrett, T., Guingab-Cagmat, J., Meshinchi, S. & Lamba, J. Distinct Metabolic features differentiating FLT3-ITD AML from FLT3-WT childhood Acute Myeloid Leukemia. *Sci Rep* **8**, 5534 (2018). https://doi.org/10.1038/s41598-018-23863-9

15 O'Brien, C. *et al.* Plasma lipid levels predict chemotherapy response and survival in acute myeloid leukemia. *Blood* **146**, 2589-2596 (2025). https://doi.org/10.1182/blood.2025029132

16 Pegg, A. E. Functions of Polyamines in Mammals. *J Biol Chem* **291**, 14904-14912 (2016). https://doi.org/10.1074/jbc.R116.731661

17 Nakanishi, S. *et al.* The Polyamine-Hypusine Circuit Controls an Oncogenic Translational Program Essential for Malignant Conversion in MYC-Driven Lymphoma. *Blood Cancer Discov* **4**, 294-317 (2023). https://doi.org/10.1158/2643-3230.Bcd-22-0162

18 Rondeau, V. *et al.* Spermidine metabolism regulates leukemia stem and progenitor cell function through KAT7 expression in patient-derived mouse models. *Sci Transl Med* **16**, eadn1285 (2024). https://doi.org/10.1126/scitranslmed.adn1285

19 Wallick, C. J. *et al.* Key role for p27Kip1, retinoblastoma protein Rb, and MYCN in polyamine inhibitor-induced G1 cell cycle arrest in MYCN-amplified human neuroblastoma cells. *Oncogene* **24**, 5606-5618 (2005). https://doi.org/10.1038/sj.onc.1208808

20 Khan, A. *et al.* Dual targeting of polyamine synthesis and uptake in diffuse intrinsic pontine gliomas. *Nat Commun* **12**, 971 (2021). https://doi.org/10.1038/s41467-021-20896-z

21 Kramer, D. L. *et al.* Effects of novel spermine analogues on cell cycle progression and apoptosis in MALME-3M human melanoma cells. *Cancer Res* **57**, 5521-5527 (1997).

22 O'Shaughnessy, J. A. *et al.* Alpha-difluoromethylornithine as treatment for metastatic breast cancer patients. *Clin Cancer Res* **5**, 3438-3444 (1999).

23 Casero, R. A., Murray Stewart, T. & Pegg, A. E. Polyamine metabolism and cancer: treatments, challenges and opportunities. *Nature Reviews Cancer* **18**, 681-695 (2018). https://doi.org/10.1038/s41568-018-0050-3

24 Holbert, C. E., Cullen, M. T., Casero, R. A., Jr. & Stewart, T. M. Polyamines in cancer: integrating organismal metabolism and antitumour immunity. *Nat Rev Cancer* **22**, 467-480 (2022). https://doi.org/10.1038/s41568-022-00473-2

25 Goyal, L. *et al.* Phase 1 study of N(1),N(11)-diethylnorspermine (DENSPM) in patients with advanced hepatocellular carcinoma. *Cancer Chemother Pharmacol* **72**, 1305-1314 (2013). https://doi.org/10.1007/s00280-013-2293-8

26 Hahm, H. A. *et al.* Phase I study of N(1),N(11)-diethylnorspermine in patients with non-small cell lung cancer. *Clin Cancer Res* **8**, 684-690 (2002).

27 Wolff, A. C. *et al.* A Phase II study of the polyamine analog N1,N11-diethylnorspermine (DENSpm) daily for five days every 21 days in patients with previously treated metastatic breast cancer. *Clin Cancer Res* **9**, 5922-5928 (2003).

28 Sinicrope, F. A. *et al.* Efficacy of Difluoromethylornithine and Aspirin for Treatment of Adenomas and Aberrant Crypt Foci in Patients with Prior Advanced Colorectal Neoplasms. *Cancer Prev Res (Phila)* **12**, 821-830 (2019). https://doi.org/10.1158/1940-6207.Capr-19-0167

29 Messing, E. *et al.* Randomized prospective phase III trial of difluoromethylornithine vs placebo in preventing recurrence of completely resected low risk superficial bladder cancer. *J Urol* **176**, 500-504 (2006). https://doi.org/10.1016/j.juro.2006.03.061

30 Bennett, J. *et al.* Paralog-specific signaling by IRAK1/4 maintains MyD88-independent functions in MDS/AML. *Blood* **142**, 989-1007 (2023). https://doi.org/10.1182/blood.2022018718

31 Ge, S. X., Jung, D. & Yao, R. ShinyGO: a graphical gene-set enrichment tool for animals and plants. *Bioinformatics* **36**, 2628-2629 (2020). https://doi.org/10.1093/bioinformatics/btz931

32 Huang, K. *et al.* Autonomous biomedical research with an artificial intelligence agent. *Science* **0**, eadz4351 https://doi.org/doi:10.1126/science.adz4351

33 Novita Sari, I. *et al.* Metabolism and function of polyamines in cancer progression. *Cancer Letters* **519**, 91-104 (2021). https://doi.org/https://doi.org/10.1016/j.canlet.2021.06.020

34 Kang, H. A. & Hershey, J. W. Effect of initiation factor eIF-5A depletion on protein synthesis and proliferation of Saccharomyces cerevisiae. *J Biol Chem* **269**, 3934-3940 (1994).

35 Henderson, A. & Hershey, J. W. Eukaryotic translation initiation factor (eIF) 5A stimulates protein synthesis in Saccharomyces cerevisiae. *Proceedings of the National Academy of Sciences* **108**, 6415-6419 (2011). https://doi.org/doi:10.1073/pnas.1008150108

36 Saini, P., Eyler, D. E., Green, R. & Dever, T. E. Hypusine-containing protein eIF5A promotes translation elongation. *Nature* **459**, 118-121 (2009). https://doi.org/10.1038/nature08034

37 Park, M. H. & Wolff, E. C. Hypusine, a polyamine-derived amino acid critical for eukaryotic translation. *Journal of Biological Chemistry* **293**, 18710-18718 (2018). https://doi.org/https://doi.org/10.1074/jbc.TM118.003341

38 Antony, C. *et al.* Control of ribosomal RNA synthesis by hematopoietic transcription factors. *Mol Cell* **82**, 3826-3839.e3829 (2022). https://doi.org/10.1016/j.molcel.2022.08.027

39 . (!!! INVALID CITATION !!! 18).

40 Sun, F. *et al.* Ara-c induces cell cycle G1/S arrest by inducing upregulation of the INK4 family gene or directly inhibiting the formation of the cell cycle-dependent complex CDK4/cyclin D1. *Cell Cycle* **18**, 2293-2306 (2019). https://doi.org/10.1080/15384101.2019.1644913

41 Yang, C. *et al.* CDK4/6 Inhibitor PD 0332991 Sensitizes Acute Myeloid Leukemia to Cytarabine-Mediated Cytotoxicity. *Cancer Res* **75**, 1838-1845 (2015). https://doi.org/10.1158/0008-5472.Can-14-2486

42 Van Linden, A. A. *et al.* Inhibition of Wee1 sensitizes cancer cells to antimetabolite chemotherapeutics in vitro and in vivo, independent of p53 functionality. *Mol Cancer Ther* **12**, 2675-2684 (2013). https://doi.org/10.1158/1535-7163.Mct-13-0424

43 Chaudhary, S. *et al.* Mitochondrial complex II and V activity is enhanced in pediatric acute myeloid leukemia. *Am J Blood Res* **11**, 534-543 (2021).

44 Tan, T. C. J. *et al.* Translation factor eIF5a is essential for IFNγ production and cell cycle regulation in primary CD8+ T lymphocytes. *Nature Communications* **13**, 7796 (2022). https://doi.org/10.1038/s41467-022-35252-y

45 Jiang, R. *et al.* Activation of polyamine catabolism by N1, N11-diethylnorspermine alters the cellular localization of mTOR and downregulates mTOR protein level in glioblastoma cells. *Cancer Biol Ther* **6**, 1644-1648 (2007). https://doi.org/10.4161/cbt.6.10.4800

Figure Legends

Fig. 1. Polyamine depletion targets pediatric AML cells. (A) Colony-forming ability of eight pediatric AML PDX specimens following 24 h treatment with 10 μM DENSpm or vehicle. Colony numbers were quantified 14–21 days post-plating. Statistical significance was determined using multiple unpaired t-tests. **(B)** Colony-forming ability of eight pediatric AML PDX specimens following 24 h treatment with 2.5 mM DFMO, 400 nM AMXT-1501, DFMO + AMXT-1501 (2.5 mM and 400 nM, respectively), or vehicle. Colony numbers were quantified 14–21 days post-plating. Statistical significance was determined using two-way ANOVA. **(C)** Experimental design of *in vivo* DENSpm treatment and leukemic burden in NSG-S mice. Two pediatric AML PDX specimens (AML5 and AML6) were transplanted into NSG-S mice. Mice were treated with DENSpm (60 mg/kg) or vehicle 5 days per week for 2 weeks prior to assessment of bone marrow (BM) engraftment. Each point represents a single mouse. Schematic created with BioRender.com. Statistical significance was determined using an unpaired Mann-Whitney test. All error bars represent standard deviation. *P < 0.05, **P < 0.01, ***P < 0.001, ***P < 0.0001.

Fig. 2. Polyamine depletion and eIF5A hypusination inhibition reduce protein synthesis in pediatric AML. (A) Relative puromycin incorporation in $CD34^+$ LSCs enriched from three pediatric AML PDX specimens (AML1, AML2, and AML3) following 24 h treatment with 10 μM DENSpm, 2.5 mM DFMO + 400 nM AMXT-1501, or vehicle, as determined by flow cytometry. Statistical significance was determined using one-way ANOVA. **(B)** Expression of hypusinated eIF5A ($eIF5A^H$) and FLAG in MOLM-13 cells expressing empty vector, wild-type eIF5A, or hypusination-defective eIF5A mutant in combination with non-targeting control or eIF5A-targeting shRNA, as determined by Western blot. **(C)** Colony-forming ability of MOLM-13 cells expressing empty vector, wild-type eIF5A, or hypusination-defective eIF5A mutant in combination with non-targeting control or eIF5A-targeting shRNA. Cells were selected with puromycin for 48 h, and colony-forming assays were performed 72 h after puromycin withdrawal. Statistical significance

was determined using one-way ANOVA. **(D)** Relative puromycin incorporation in $CD34^+$ LSCs enriched from three pediatric AML PDX specimens (AML1, AML2, and AML3) following 24 h treatment with 25–50 μM GC7 or vehicle, as determined by flow cytometry. Statistical significance was determined using an unpaired t-test. **(E)** Colony-forming ability of eight pediatric AML PDX specimens following treatment with vehicle, with 50 μM GC7 added directly to the MethoCult medium. Colony numbers were quantified 14–21 days post-plating. Statistical significance was determined using multiple unpaired t-tests. **(F)** Colony-forming ability of CD34+ selected cord blood cells following treatment with vehicle or 50 μM GC7. Colonies were counted 14 days post plating. Statistical significance was determined using an unpaired t-test. All error bars represent standard deviation. ns, not significant; *P < 0.05, **P < 0.01, ***P < 0.001, ***P < 0.0001.

Fig. 3. Polyamine depletion and eIF5A hypusination inhibition reduce the expression of cell cycle related proteins. (A) Schematic of the experimental design. Three pediatric PDX specimens were treated with DENSpm or GC7 for 24 h, collected, and subjected to proteomics analysis. Schematic created with BioRender.com. **(B)** Volcano plots showing differential protein expression in pediatric AML PDX cells following treatment with DENSpm or GC7 compared to vehicle-treated cells. **(C)** Venn diagram comparing differentially expressed proteins following DENSpm and GC7 treatment. Proteins with P < 0.05 in a paired t-test were considered significantly altered. **(D)** Heatmap of significantly altered expression following DENSpm and GC7 treatment relative to vehicle-treated controls. **(E)** KEGG pathway analysis of the shared changes in protein expression.

Fig. 4 Polyamine depletion and eIF5A hypusination inhibition result in reduced translation of cell cycle related mRNAs. (A) PCA of differentially translated mRNAs. (**B)** Volcano plots of differentially expressed mRNAs in the ribosome sequencing that were not altered at the gene

expression level (unique DEGs). **(C)** Pathway analysis of differentially translated mRNAs with cell cycle related pathways highlighted.

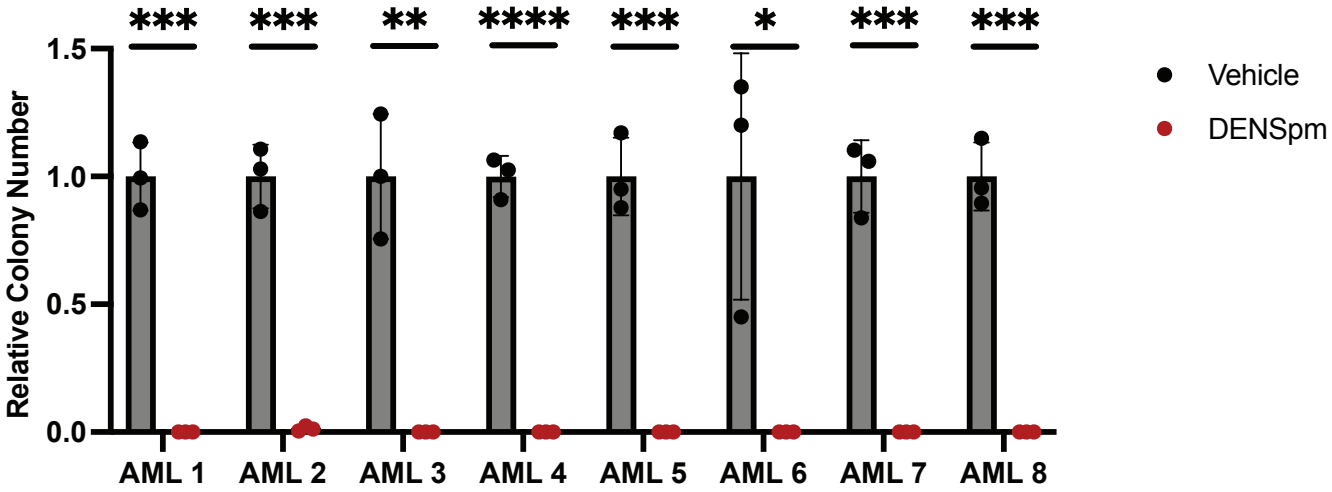
Fig. 5. Polyamine depletion and eIF5A hypusination inhibition result in a G_1 cell cycle arrest. (A) Representative flow cytometry analysis of EdU and DAPI staining in a pediatric AML PDX specimen following 24 h treatment with 10 μM DENSpm, 50 μM GC7, or vehicle. **(B)** Percentage of cells in each cell-cycle phase determined by EdU incorporation and DAPI staining in three pediatric AML PDX specimens (AML1, AML2, and AML3) following 24 h treatment with 10 μM DENSpm, 50 μM GC7, or vehicle, as determined by flow cytometry. Statistical significance was determined using two-way ANOVA. **(C)** Relative puromycin incorporation in G1 and S/G2/M cell populations from three pediatric AML PDX specimens (AML1, AML2, AML3) following 24 h treatment with 10 μM DENSpm, 25–50 μM GC7, or vehicle, as determined by flow cytometry. Statistical significance was determined using one-way ANOVA. **(D)** Percentage of cells in early apoptosis (Annexin V^+ $DAPI^-$) and late apoptosis (Annexin V^+ $DAPI^+$) in three pediatric AML PDX specimens (AML1, AML2, and AML3) following 48 h treatment with 10 μM DENSpm, 50 μM GC7, or vehicle, as determined by flow cytometry. Statistical significance was determined based on total apoptotic cells using one-way ANOVA. All error bars represent standard deviation. ns, not significant; *P < 0.05, **P < 0.01, ***P < 0.001, ***P < 0.0001.

Fig. 6. Polyamine depletion sensitizes pediatric AML PDX cells to chemotherapy. (A) Viability of three pediatric AML PDX specimens (AML1, AML2, and AML3) following 48 h treatment with 2.5 μM DENSpm, 1.25 μM cytarabine, DENSpm + cytarabine (2.5 μM and 1.25 μM, respectively), or vehicle. Statistical significance was determined using one-way ANOVA. **(B)** Colony-forming ability of three pediatric AML PDX specimens (AML1, AML2, and AML3) following 24 h treatment with 2.5 μM DENSpm, 1.25 μM cytarabine, DENSpm + cytarabine (2.5 μM and 1.25 μM, respectively), or vehicle. Colony numbers were quantified 14–21 days post-plating. **(C)**

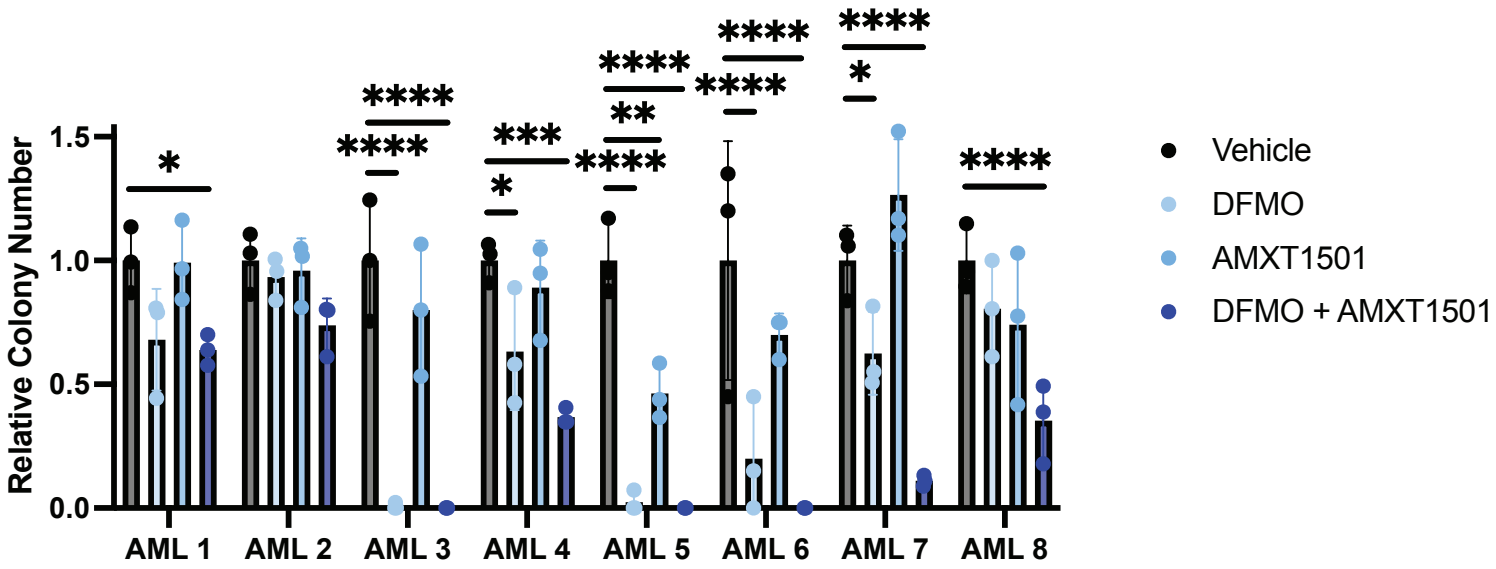
Bone marrow burden in mice following a 2-week treatment with vehicle, DENSpm, chemotherapy, or the combination of DENSpm and chemotherapy. Bone marrow aspirates were measured 45 and 56 days post-treatment. **(D)** Survival of mice treated with vehicle, DENSpm, chemotherapy, or the combination of DENSpm and chemotherapy. Statistical significance was determined using one-way ANOVA. All error bars represent standard deviation. ns, not significant; *P < 0.05, **P < 0.01, ***P < 0.001, ***P < 0.0001.

Figure 1

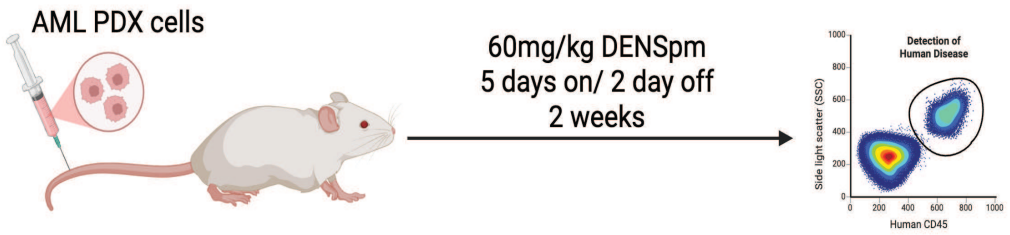
A.


***
***
**
****
***
*
***
***
1.5
1.0
0.5
0.0
Relative Colony Number
AML 1
AML 2
AML 3
AML 4
AML 5
AML 6
AML 7
AML 8
Vehicle
DENSpm

B.


*
****
****
***
*
****
**
****
****
****
*
****
1.5
1.0
0.5
0.0
Relative Colony Number
AML 1
AML 2
AML 3
AML 4
AML 5
AML 6
AML 7
AML 8
Vehicle
DFMO
AMXT1501
DFMO + AMXT1501

C.


AML PDX cells
60mg/kg DENSpm
5 days on/ 2 day off
2 weeks
Detection of Human Disease
Side light scatter (SSC)
Human CD45

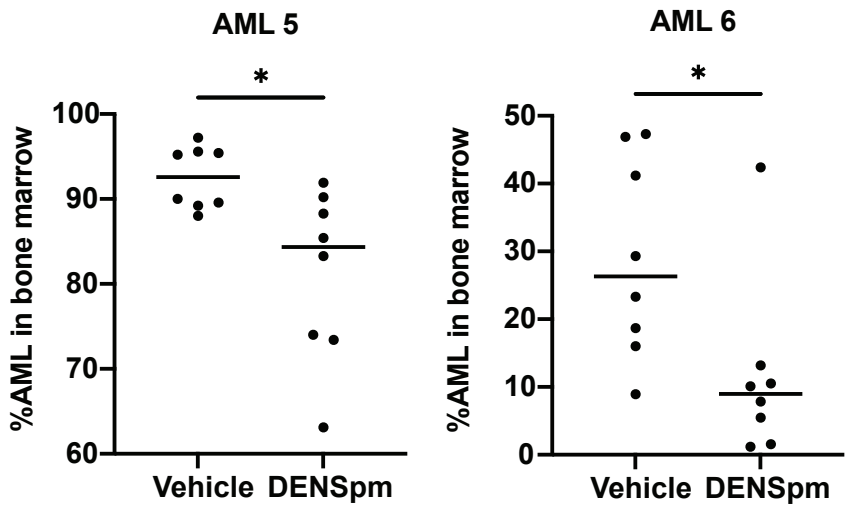

AML 5
*
100
90
80
70
60
%AML in bone marrow
Vehicle
DENSpm
AML 6
*
50
40
30
20
10
0
%AML in bone marrow
Vehicle
DENSpm

Figure 2

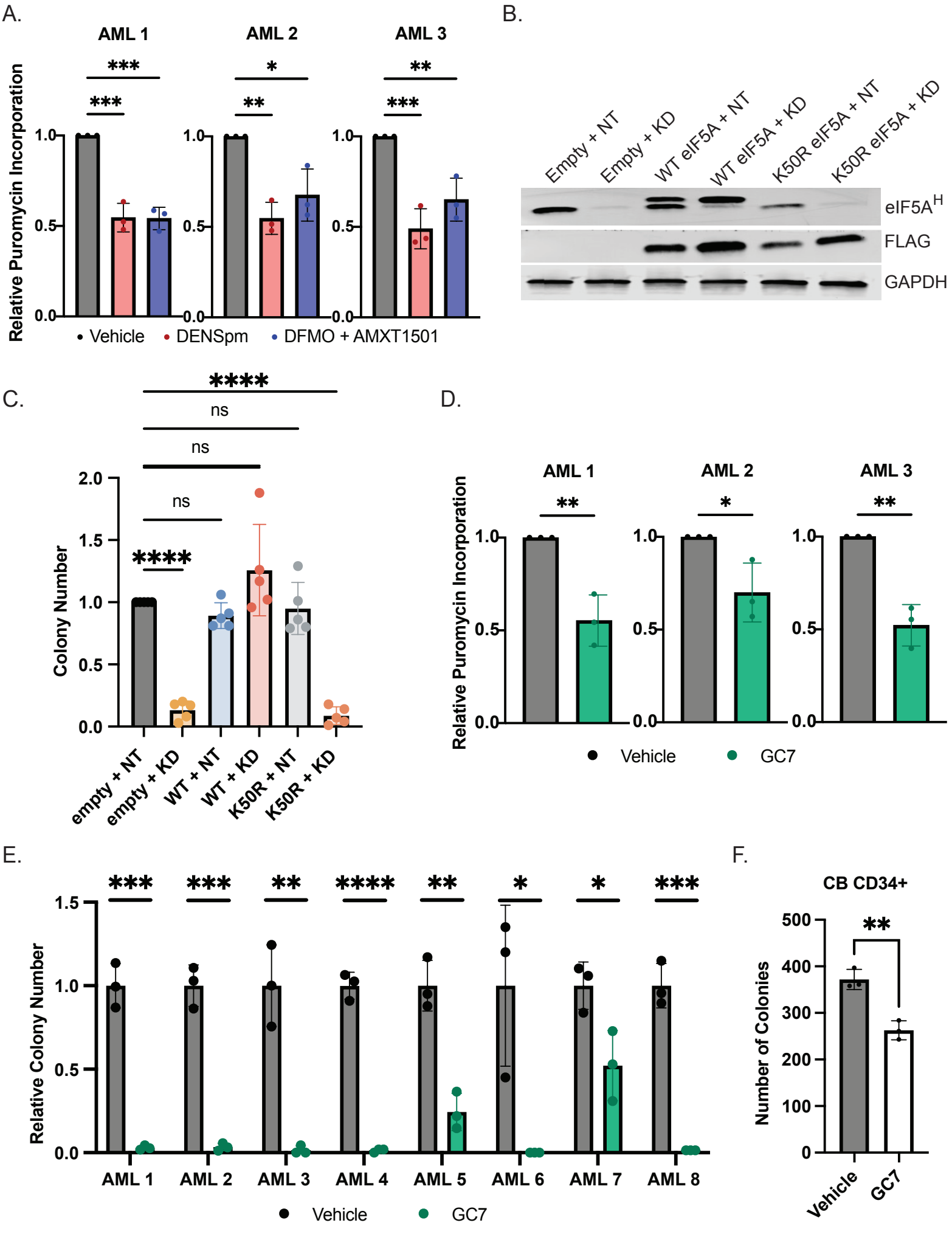

A.
AML 1
AML 2
AML 3
***
***
*
**
**
***
Relative Puromycin Incorporation
1.0
0.5
0.0
• Vehicle
• DENSpm
• DFMO + AMXT1501
B.
Empty + NT
Empty + KD
WT eIF5A + NT
WT eIF5A + KD
K50R eIF5A + NT
K50R eIF5A + KD
eIF5A^H
FLAG
GAPDH
C.
****
ns
ns
ns
****
Colony Number
2.0
1.5
1.0
0.5
0.0
empty + NT
empty + KD
WT + NT
WT + KD
K50R + NT
K50R + KD
D.
AML 1
AML 2
AML 3
**
*
**
Relative Puromycin Incorporation
1.0
0.5
0.0
Vehicle
GC7
E.
***
***
**
****
**
*
*
***
Relative Colony Number
1.5
1.0
0.5
0.0
AML 1
AML 2
AML 3
AML 4
AML 5
AML 6
AML 7
AML 8
Vehicle
GC7
F.
CB CD34+
**
Number of Colonies
500
400
300
200
100
0
Vehicle
GC7

Figure 3

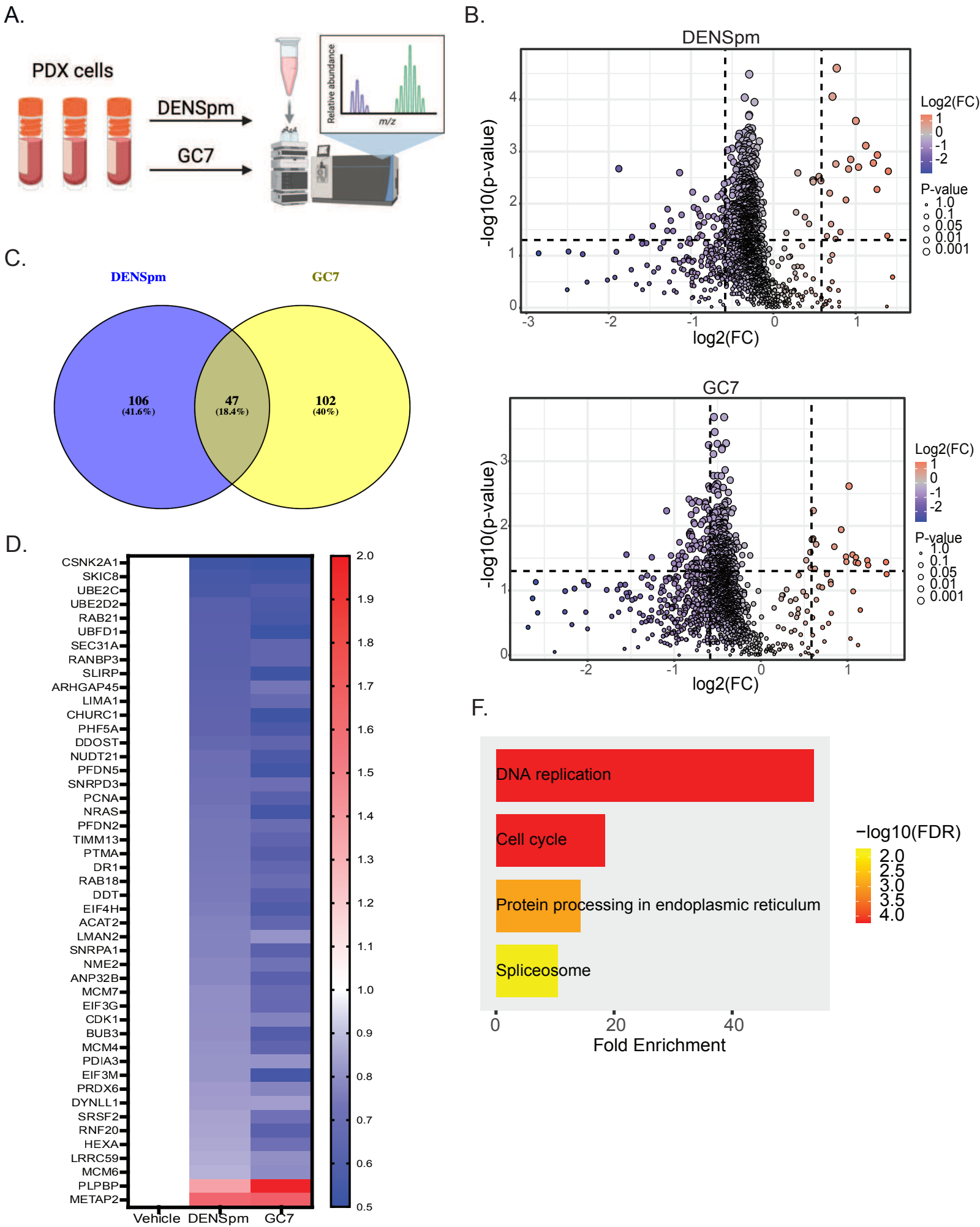
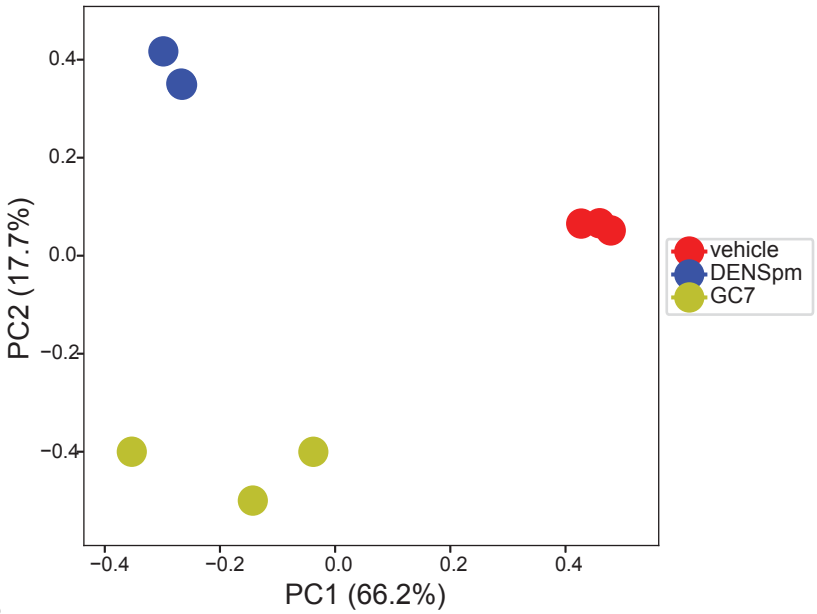
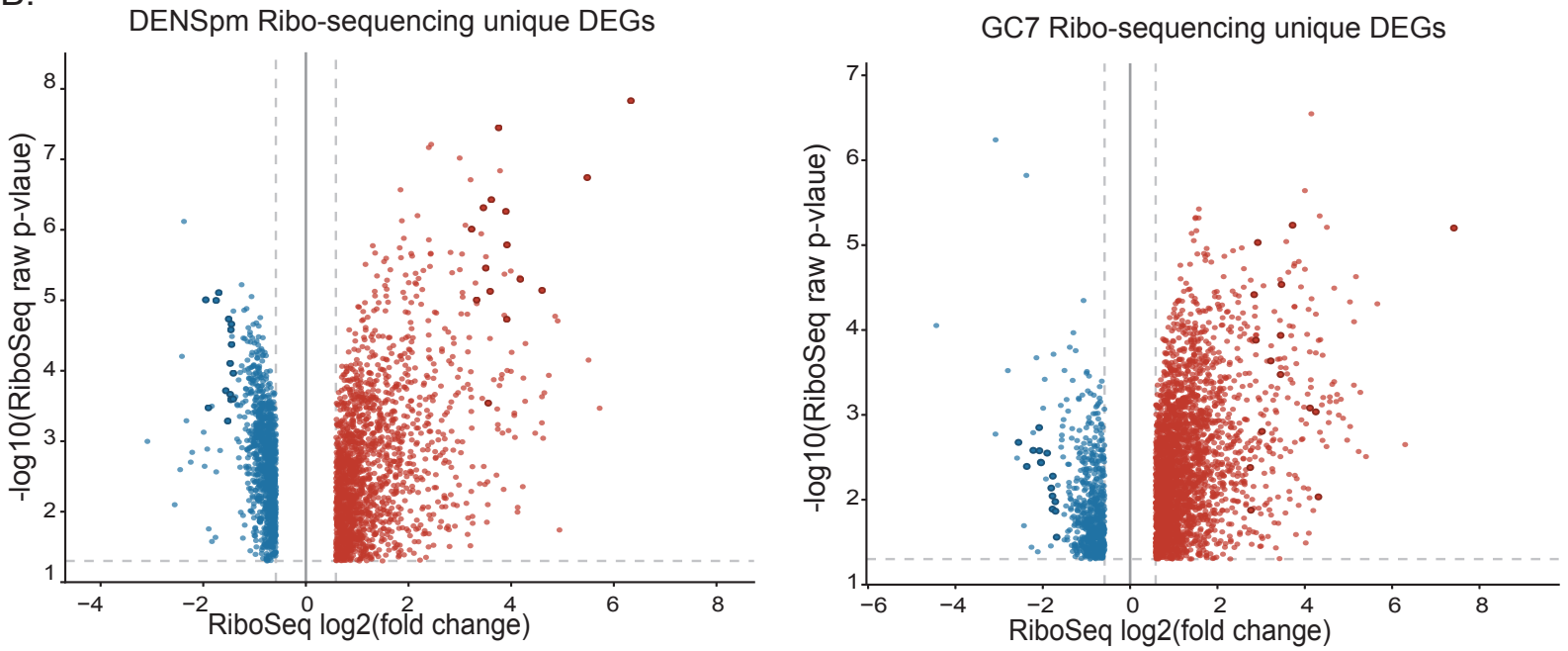

A.
PDX cells
DENSpm
GC7
Relative abundance
m/z
B.
DENSpm
-log10(p-value)
log2(FC)
Log2(FC)
P-value
GC7
C.
DENSpm
GC7
106
(41.6%)
47
(18.4%)
102
(40%)
D.
CSNK2A1
SKIC8
UBE2C
UBE2D2
RAB21
UBFD1
SEC31A
RANBP3
SLIRP
ARHGAP45
LIMA1
CHURC1
PHF5A
DDOST
NUDT21
PFDN5
SNRPD3
PCNA
NRAS
PFDN2
TIMM13
PTMA
DR1
RAB18
DDT
EIF4H
ACAT2
LMAN2
SNRPA1
NME2
ANP32B
MCM7
EIF3G
CDK1
BUB3
MCM4
PDIA3
EIF3M
PRDX6
DYNLL1
SRSF2
RNF20
HEXA
LRRC59
MCM6
PLPBP
METAP2
Vehicle
DENSpm
GC7
F.
DNA replication
Cell cycle
Protein processing in endoplasmic reticulum
Spliceosome
Fold Enrichment
−log10(FDR)

Figure 4

A.


PC2 (17.7%)
PC1 (66.2%)
vehicle
DENSpm
GC7

B.


DENSpm Ribo-sequencing unique DEGs
GC7 Ribo-sequencing unique DEGs
-log10(RiboSeq raw p-vlaue)
RiboSeq log2(fold change)

C.

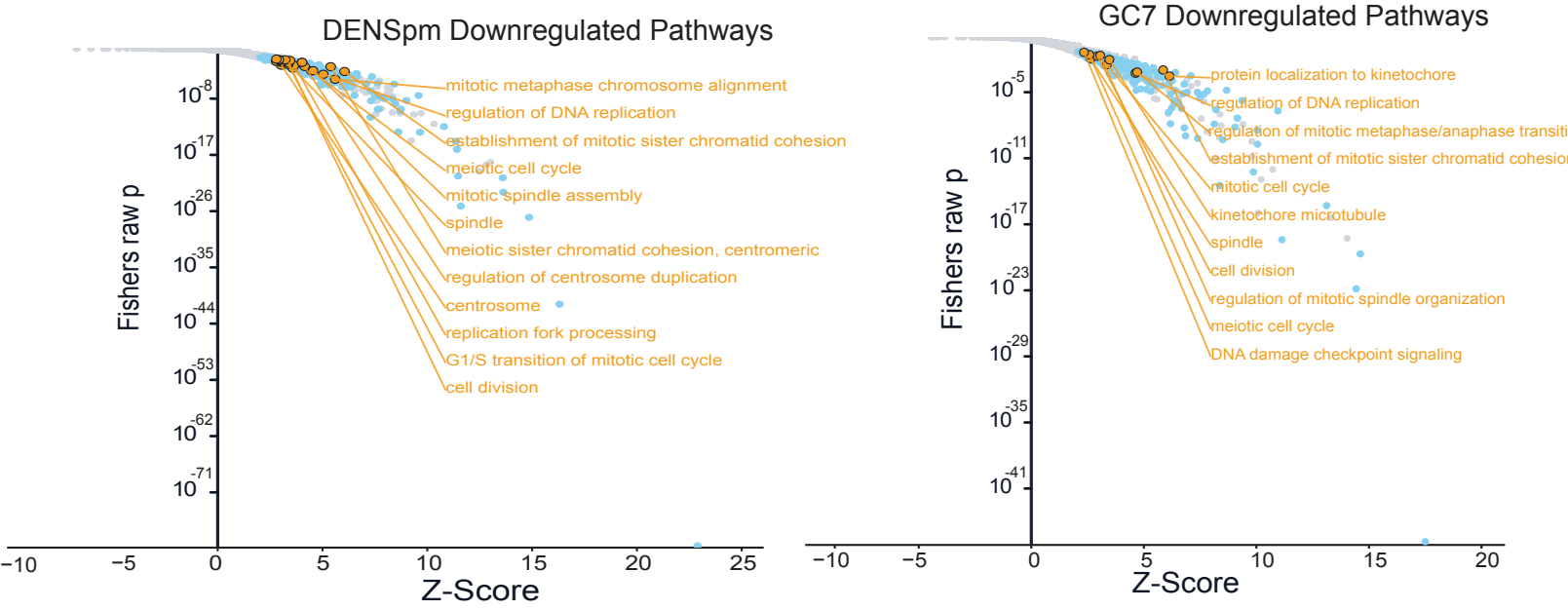
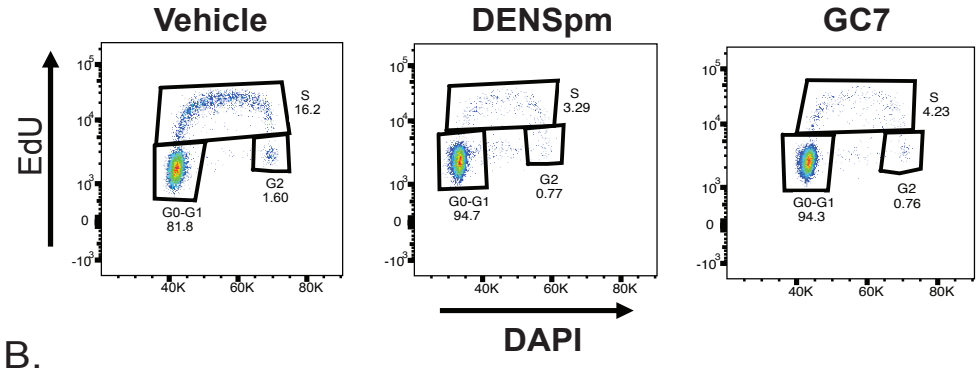
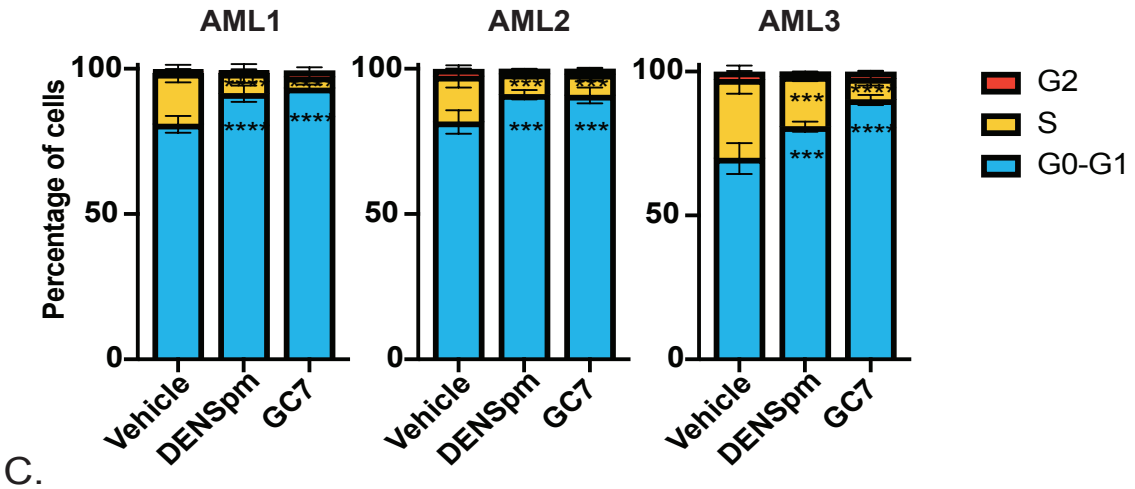

DENSpm Downregulated Pathways
mitotic metaphase chromosome alignment
regulation of DNA replication
establishment of mitotic sister chromatid cohesion
meiotic cell cycle
mitotic spindle assembly
spindle
meiotic sister chromatid cohesion, centromeric
regulation of centrosome duplication
centrosome
replication fork processing
G1/S transition of mitotic cell cycle
cell division
GC7 Downregulated Pathways
protein localization to kinetochore
regulation of DNA replication
regulation of mitotic metaphase/anaphase transition
establishment of mitotic sister chromatid cohesion
mitotic cell cycle
kinetochore microtubule
spindle
cell division
regulation of mitotic spindle organization
meiotic cell cycle
DNA damage checkpoint signaling
Fishers raw p
Z-Score

Figure 5

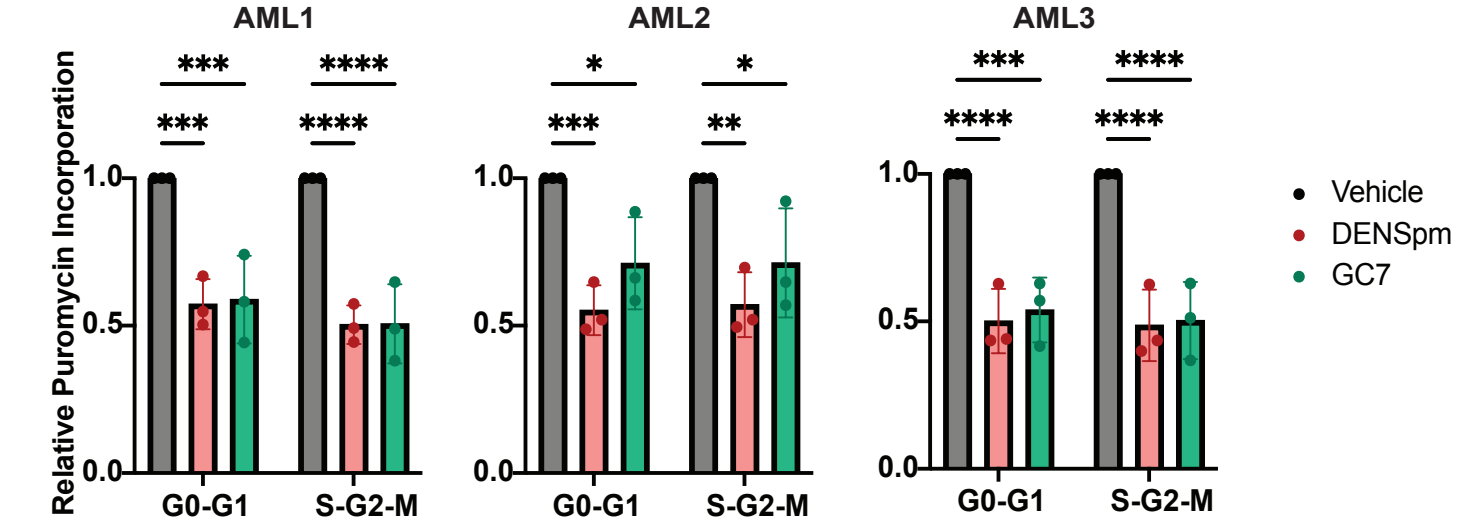
A.



B.



C.



D.

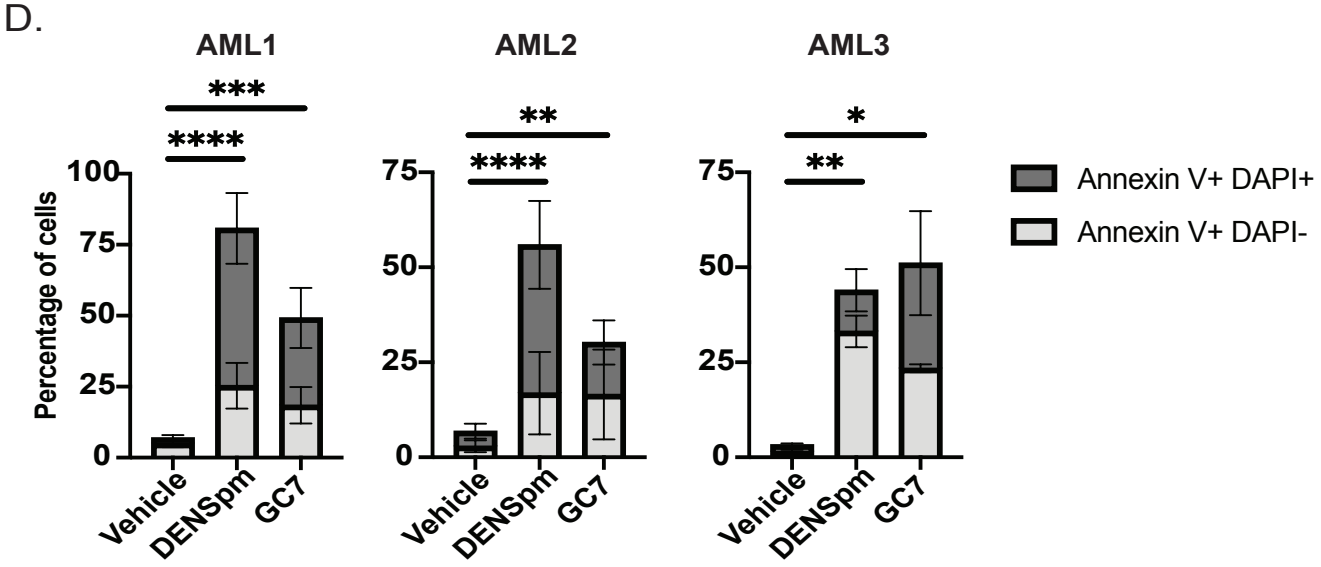
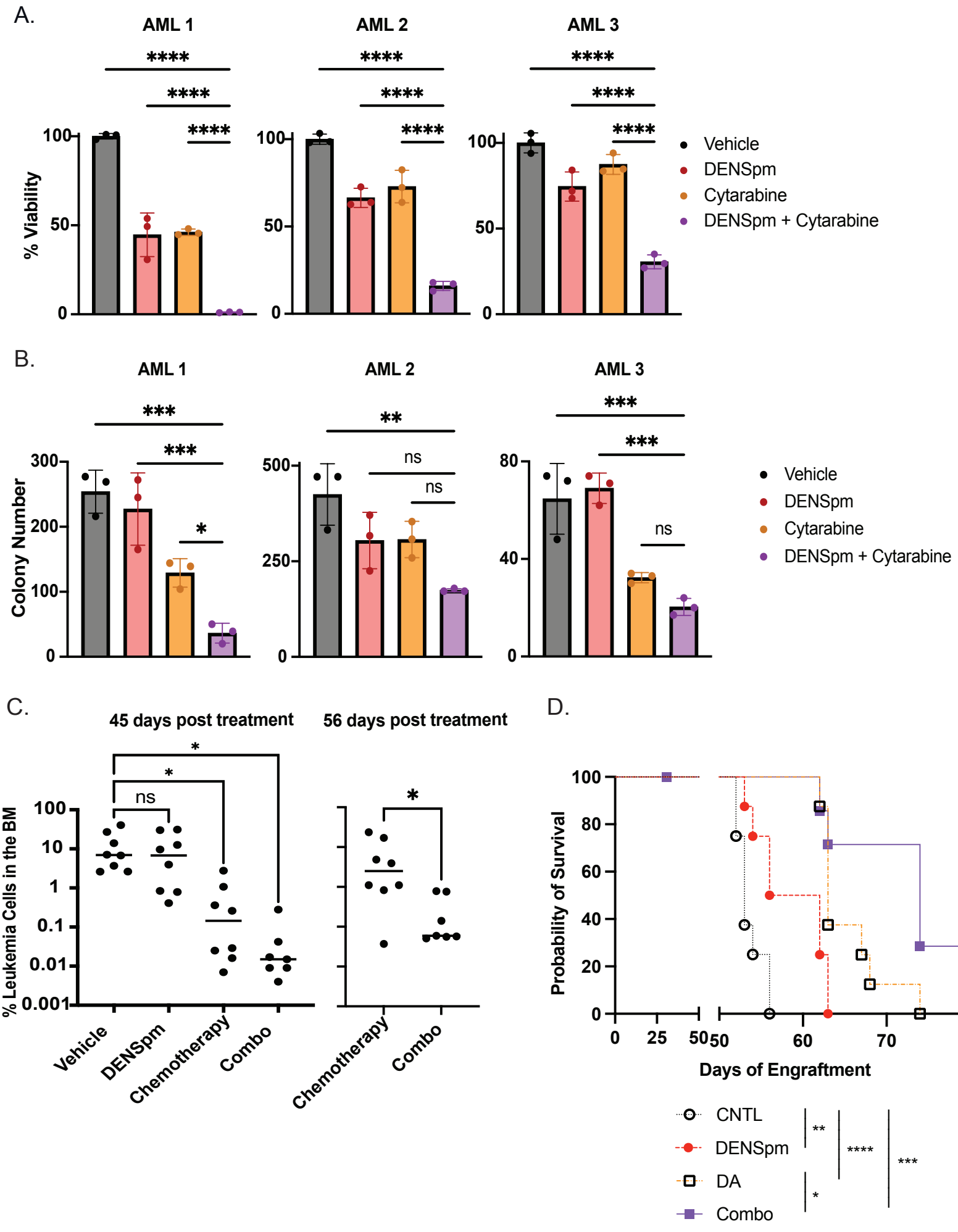


Figure 6


A.
AML 1
AML 2
AML 3
****
% Viability
100
50
0
Vehicle
DENSpm
Cytarabine
DENSpm + Cytarabine
B.
AML 1
AML 2
AML 3
***
**
ns
*
Colony Number
300
200
100
500
250
80
40
C.
45 days post treatment
56 days post treatment
% Leukemia Cells in the BM
100
10
1
0.1
0.01
0.001
Vehicle
DENSpm
Chemotherapy
Combo
D.
Probability of Survival
Days of Engraftment
CNTL
DENSpm
DA
Combo

Supplementary Files

This is a list of supplementary files associated with this preprint. Click to download.

- TableS1.xlsx
- SupplementaryFiles.pdf